41st AIAA/ASME/SAE/ASEE Joint Propulsion Conference & Exhibit, 10 - 13 Jul 2005, Tucson, Arizona

Numerical Analysis of Free Molecule Micro-Resistojet Performance

Zeeshan Ahmed* and Sergey F. Gimelshein†

University of Southern California, Los Angeles, CA 90089

Andrew D. Ketsdever‡

Air Force Research Laboratory, Propulsion Directorate, Edwards AFB, California

I. Introduction

One of the most crucial requirements of modern space missions is the miniaturization of spacecraft and satellites. The miniaturization is tightly connected with new space technologies promoted by the Air Force, DARPA, and NASA, such as spacecraft formation flying, that implies two or more spacecraft that operate synchronously in a controlled spatial configuration. This, in turn, necessitates the development of new propulsion systems able to deliver precise impulse bits while meeting strict mass, size and power usage limitations.

Currently, various micropropulsion concepts are being considered, such as cold gas,[1] catalytic decomposition,[2] mono- and bi-propellant[3] thrusters. For most micropropulsion devices, the fluid mechanics of reduced length scales (low Reynolds numbers) dictates that there will be a significant degradation of the thrust efficiency due to increased viscous and heat transfer losses. Both experimental and numerical investigation of fluid flow and performance of microthrusters is necessary for realistic evaluation of advantages and drawbacks of the new micropropulsion concepts.

In this work, a Free Molecule Micro-Resistojet (FMMR) is examined numerically, that was developed and described in Ref.,[4] and recently studied experimentally in Ref.[5] The FMMR is an electrothermal propulsion system designed for on-orbit maneuvers of nanospacecraft (mass 10 kg). The FMMR is being developed[5] to fly on a Texas A&M (TAM)nanosatellite. This nanosatellite flight will investigate the survivability and capability of water propelled micro-thrusters for attitude control maneuvers on a small satellite and could also mark the first operation of a MEMS fabricated thruster in space. The delivered thruster system will operate on the vapor pressure of water, stored in either a liquid or solid state (depending on the internal satellite temperature). The FMMR will provide a de-spin capability for the nanosatellite to allow proper positioning of the satellite.

The propellant gas, originating from a propellant tank and passing through hydrophobic microporous membrane filters and a valve, enters the base of a Teflon plenum through an inlet. The hydrophobic microporous membrane uses the surface tension of the propellant to serve as a phase separator, allowing only the propellant vapor to pass through. The FMMR heater chip shown in Fig. 1 (left) is attached to the top of the plenum. Propellant molecules gain kinetic energy as they collide with heated walls of the expansion slots. The increase in kinetic energy of the propellant molecules is critical to the performance and operation of the FMMR. Due to the inherently low operating pressures of the FMMR, the propellant molecules are heated only through the direct interaction with the expansion slots, as intermolecular collisions are negligible.[4]

*Undergraduate Research Assistant, Department of Aerospace and Mechanical Engineering.

†Research Assistant Professor, Department of Aerospace and Mechanical Engineering, Member AIAA.

‡Group Leader, Senior Member AIAA.

Report Documentation Page

Form Approved
OMB No. 0704-0188

1. REPORT DATE	2. REPORT TYPE	3. DATES COVERED
JUN 2005		-

4. TITLE AND SUBTITLE	5a. CONTRACT NUMBER
Numerical Analysis of Free Molecule Micro-Resistojet Performance	5b. GRANT NUMBER
	5c. PROGRAM ELEMENT NUMBER

6. AUTHOR(S)	5d. PROJECT NUMBER
Zeeshan Ahmed; Sergey Gimelshein; Andrew Ketsdever	**5026**
	5e. TASK NUMBER **0568**
	5f. WORK UNIT NUMBER

7. PERFORMING ORGANIZATION NAME(S) AND ADDRESS(ES)	8. PERFORMING ORGANIZATION REPORT NUMBER
Air Force Research Laboratory (AFMC),AFRL/PRSA,10 E. Saturn Blvd.,Edwards AFB,CA,93524-7680	

9. SPONSORING/MONITORING AGENCY NAME(S) AND ADDRESS(ES)	10. SPONSOR/MONITOR'S ACRONYM(S)
	11. SPONSOR/MONITOR'S REPORT NUMBER(S)

12. DISTRIBUTION/AVAILABILITY STATEMENT

Approved for public release; distribution unlimited

13. SUPPLEMENTARY NOTES

14. ABSTRACT

One of the most crucial requirements of modern space missions is the miniaturization of spacecraft and satellites. The miniaturization is tightly connected with new space technologies promoted by the Air Force DARPA, and NASA, such as spacecraft formation ying, that implies two or more spacecraft that operate synchronously in a controlled spatial con guration. This, in turn, necessitates the development of new propulsion systems able to deliver precise impulse bits while meeting strict mass, size and power usage limitations. Currently, various micropropulsion concepts are being considered, such as cold gas,1 catalytic decomposition 2 mono- and bi-propellant3 thrusters. For most micropropulsion devices, the uid mechanics of reduced length scales (low Reynolds numbers) dictates that there will be a signi cant degradation of the thrust e ciency due to increased viscous and heat transfer losses. Both experimental and numerical investigation of uid ow and performance of microthrusters is necessary for realistic evaluation of advantages and drawbacks of the new micropropulsion concepts. In this work, a Free Molecule Micro-Resistojet (FMMR) is examined numerically, that was developed and described in Ref.,4 and recently studied experimentally in Ref.5 The FMMR is an electrothermal propulsion system designed for on-orbit maneuvers of nanospacecraft (mass 10 kg). The FMMR is being developed5 to y on a Texas A&M (TAM)nanosatellite. This nanosatellite ight will investigate the survivability and capability of water propelled micro-thrusters for attitude control maneuvers on a small satellite and could also mark the rst operation of a MEMS fabricated thruster in space. The delivered thruster system will operate on the vapor pressure of water, stored in either a liquid or solid state (depending on the internal satellite temperature). The FMMR will provide a de-spin capability for the nanosatellite to allow proper positioning of the satellite.

15. SUBJECT TERMS					
16. SECURITY CLASSIFICATION OF:			17. LIMITATION OF ABSTRACT	18. NUMBER OF PAGES	19a. NAME OF RESPONSIBLE PERSON
a. REPORT **unclassified**	b. ABSTRACT **unclassified**	c. THIS PAGE **unclassified**		**11**	

Standard Form 298 (Rev. 8-98)
Prescribed by ANSI Std Z39-18

Figure 1. FMMR heater chip (left) and the plenum with the chip (right).

The FMMR exhibits many systems features that are beneficial to small satellite operations such as low cost, low power consumption, low mass, and low propellant storage volume. The FMMR operates at relatively low stagnation pressure to take advantage of the high storage density of liquid and solid propellants. By operating on the vapor pressure of the stored propellant, the FMMR reduces the amount of power required over thrusters that pre-vaporize the propellant to create high stagnation pressures. The simple design of the FMMR allows for low-cost manufacturing and testing. The FMMR heater chip allows for large ranges of thrust levels without a significant loss in performance by varying the number and dimensions of the expansion slots.

The main objectives of this work are to evaluate the performance of the FMMR for different test gases; analyze the importance of geometrical and operational parameters such as plenum pressures and chip temperatures; and estimate the level of contamination of the spacecraft surface by propellant molecules. The typical plenum pressures are relatively low (below 1,000 Pa), and the Knudsen number based on the slot thickness is on the order of unity. The direct simulation Monte Carlo (DSMC) method has therefore been used in all computations.

II. Geometry and Flow Conditions

The current iteration of the FMMR heater chip, shown in Fig. 1 (left), was designed specifically for the TAM nanosatellite mission. This iteration of the FMMR chip is an 19.2 mm by 19.2 mm square with a thickness of 500 μm. There are 44 interior expansion slots formed in two rows. Each slot is 100 μm wide by 5.375 mm long, and are etched completely through the FMMR. The expansion slots are outlined by a serpentine heater pattern consisting of a gold current carrying layer.

The plenum is designed as a rectangular box as shown in Fig. 1 (right). The internal dimensions of the plenum are 11 mm by 11 mm by 22 mm. The propellant gas is flowing through the attached tube of 6.35 mm diameter, and the expected plenum pressure may vary from tens to hundreds Pa. While the heater chip temperature will be kept at about 573 K, the temperature of other walls of the plenum will be close to room temperature.

The current design of the satellite represents a 316 mm long hexagonal cylinder with the side width of 216 mm, with the FMMR thruster mounted on one of the plates of the hexagonal surface, close to one of the end sides. The schematic of the spacecraft, that also illustrates the triangulated model geometry used in the computations, is shown in Fig. 2 (left).

III. Numerical Approach

The DSMC-based software system SMILE[6] was used in all DSMC computations. The majorant frequency scheme[7] was used to calculate intermolecular interactions. The intermolecular potential was assumed to be a variable hard sphere.[8] Energy redistribution between the rotational and translational modes was performed in accordance with the Larsen-Borgnakke model. A temperature-dependent rotational relaxation number was used. The reflection of molecules on the surface was assumed to be diffuse with complete energy

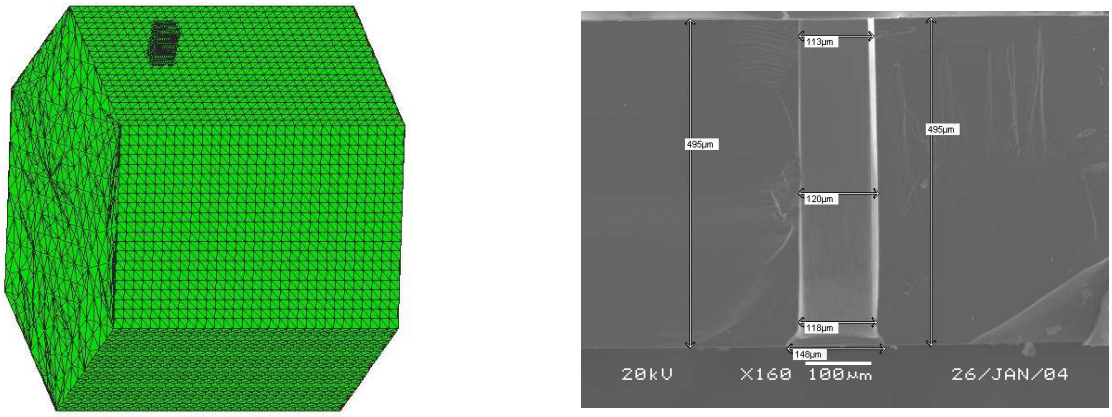

Figure 2. Satellite geometry (left) and the SEM image of a single slot of FMMR (right).

accommodation.

In order to examine the flow details both inside the plenum and near the expansion slots, as well as in the plume interacting with the spacecraft surface, the computations have been performed in three steps. The first step is the DSMC modeling of a two-dimensional flow through a single expansion slot. The etching technology used in FMMR manufacturing results in a slot geometry that is not rectangular. The first step therefore includes the actual geometry of the slot evaluated from the SEM data (the schematic of the geometry is shown in Fig. 2). The detailed modeling of the gas flow through a single slot allows for comparison of computed mass flow and thrust with available experimental data[5] for helium and nitrogen propellants. The computations are also performed for water vapor in order to analyze the actual device performance, and compare the 2D results with those obtained at the second step.

The second step includes three-dimensional modeling of the flow inside the plenum and in a small region outside of the FMMR (near field of the plume). The complex geometry of the slots is replaced by rectangular openings described in the previous section. The third step includes the modeling of the plume flow and plume impingement on spacecraft surface. A starting surface generated using the macroparameters obtained at the previous step is used. The surface is 2 cm by 2 cm and is located 0.5 mm downstream from the heater chip plane. The inflow molecules are sampled according to the corresponding ellipsoidal distribution functions.

IV. Subsonic Boundary conditions: Convergence Study

The DSMC method is conventionally used to model supersonic and hypersonic flows where the boundary conditions are either supersonic inflow or vacuum outflow. Their implementation for these cases is straightforward. For subsonic flows, such as the flow inside the plenum, the application of the DSMC method is more complicated. In the present study, the convergence study has been conducted in order to establish the minimum necessary size of the computational domain. Note that for all 2D computations zero flow velocity was assumed at the inflow boundaries, with the constant pressure and temperature corresponding to given stagnation conditions.

The convergence study has been performed for a nitrogen flow in a rectangular slot geometry. The geometry of the slot is shown in Fig. 3 where the axial velocity fields are presented for the part of the computational domain close to the slot and two lengths of plenum part, 3 mm and 5 mm. Only the top part of the flow is considered due to the symmetry of the problem. It is clearly seen that the impact of of the domain size is negligible near the slot entrance and as well as the slot exit. The more quantitative comparison is shown in Fig. 4 where the axial velocity and pressure profiles along the slot centerline are shown for the corresponding lengths of 3, 4, and 5 mm. The slot entrance is located at X=0. The difference between the three cases is within the statistical accuracy of the computations, which was a few percent for flowfields and less than a percent for integral properties, such as mass flow and thrust. These properties are summarized in Table 1. Since no visible influence of the computational domain size was observed when the subsonic chamber length was increased from 3 to 5 mm, the value of 3 mm has therefore been used hereafter.

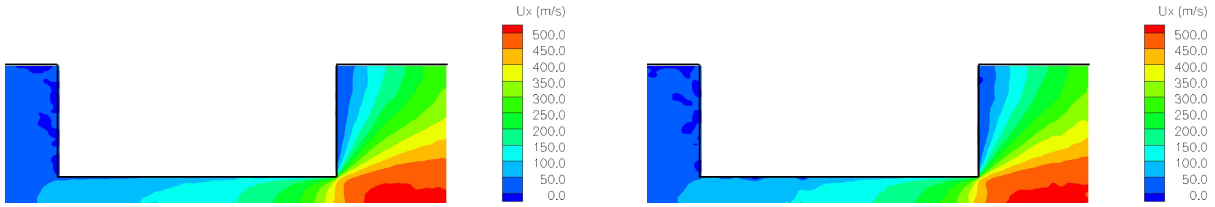

Figure 3. Axial velocity fields (m/s) inside an expansion slot for the plenum part length of 3 mm (left) and 5 mm (right).

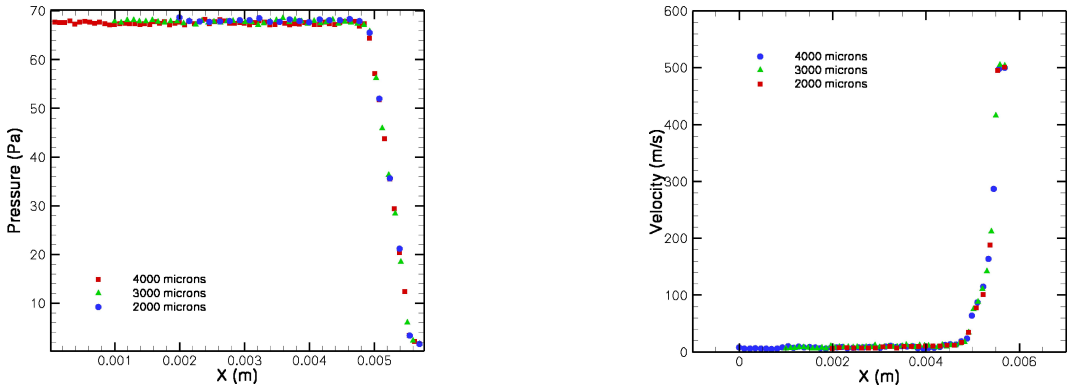

Figure 4. Axial velocity (left) and gas pressure (right) profiles along the axis of symmetry for different computational domains.

Table 1. Computational domain convergence.

Domain length, m	Mass flow, kg/s	Thrust, N
$3.0{\cdot}10^{-3}$	$5.6829{\cdot}10^{-7}$	$3.3316{\cdot}10^{-4}$
$4.0{\cdot}10^{-3}$	$5.7096{\cdot}10^{-7}$	$3.3628{\cdot}10^{-4}$
$5.0{\cdot}10^{-3}$	$5.6862{\cdot}10^{-7}$	$3.3552{\cdot}10^{-4}$

V. Effects of Chip Temperature and Stagnation Pressure on Flow Fields

The FMMR will operate at an elevated chip surface temperature of about 573 K in order to achieve acceptable efficiency of the thruster. Since the Knudsen number will be about unity based on the slot thickness, the molecule exit velocity will be primarily determined by the surface temperature, and is expected to be proportional to the square root of this temperature, T_w. The mass flow is therefore expected to be proportional to the product of the gas density near the slot exit, n_e, and $\sqrt{T_w}$, whereas the thrust is proportional to $n_e T_w$. Let us now compare the flow parameters that are important for thruster performance, the gas pressure and the axial velocity.

The influence of the chip surface temperature on gas pressure is given in Fig. 5 for nitrogen propellant. The pressure values here are normalized by the plenum value. These results show that the impact of temperature on pressure is very small both near the slot entrance and exit. Note that the gas temperature near and inside the slot was found to be close to the surface temperature in these cases, whereas the gas density inside the slot normalized by the plenum value is not affected by the surface temperature.

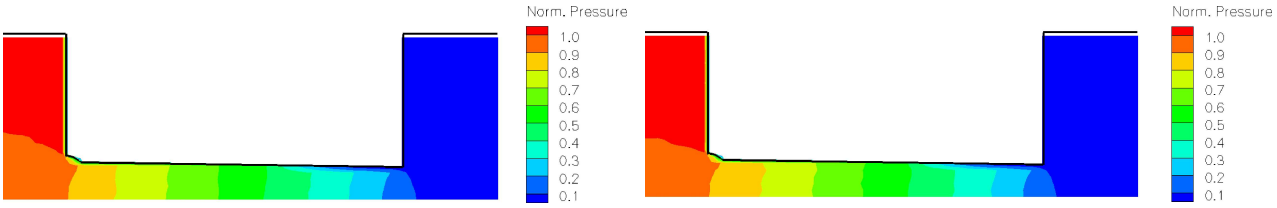

Figure 5. Normalized pressure fields for $P_0 = 49$ Pa and the chip temperature of 300 K (left) and 573 K (right).

The flow velocity however changes significantly with temperature, as illustrated in Fig. 6. The velocity reaches 50 m/s inside the slot for 300 K case and upstream from the slot entrance for 573 K. The magnitude of the difference increases toward the slot exit, and reaches over 100 m/s for the gas that leaves the slot (280 m/s for 300 K and almost 400 m/s for 573 K). This increase is nearly proportional to $\sqrt{T_w}$. Not that this proportionality may be expected for a long channel and near free-molecule flow; it is not obvious however for a finite slot length-to-thickness ratio of 5 and a Knudsen number of one for T=300 K. In the latter case there are two more contributing sources that complicate the analysis: molecules that come directly from the plenum increase the average velocity, while molecules that collide with other molecules generally decrease it. If these sources are small compared to the main surface-generated source, or if they compensate each other, the velocity will be proportional to $\sqrt{T_w}$.

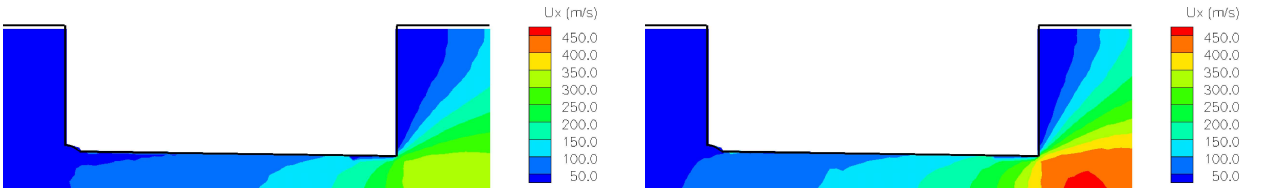

Figure 6. Axial velocity (m/s) fields for $P_0 = 49$ Pa and the chip temperature of 300 K (left) and 573 K (right).

The results of the computation for a higher pressure of 185 Pa are presented in Fig. 7. Comparison of the pressure field normalized by its plenum value with the corresponding field for 49 Pa shows that an almost four-fold increase in pressure does not change the flow pattern. Although the molecular collisions inside the slot become likely as the mean free path becomes one-forth of the slot diameter, the length of the slot is still sufficient to increase velocities of most particles coming through it. The average exit velocities are almost identical for 49 Pa and 185 Pa (cf. Figs. 6 and 7).

VI. FMMR Performance and Comparison with Experimental Data

Consider now the performance characteristics of a single FMMR slot for various gas pressures and surface temperatures. The mass flow, thrust, and specific impulse are listed in Table 2 for a nitrogen flow. For all cases under consideration, the mass flow monotonously decreases when surface temperature increases. This increase is nearly proportional to $\sqrt{T_w}$; some deviation from the proportionality is related primarily to the

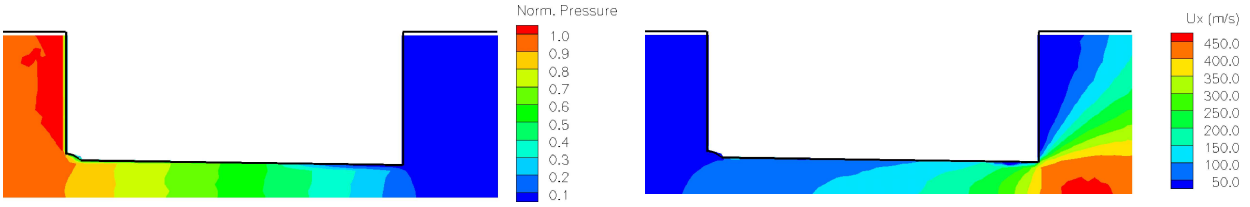

Figure 7. Normalized pressure (left) and axial velocity (right) fields for $P_0 = 185$ Pa and the chip temperature of 573 K.

effect of gas-gas collisions inside the slot; there is also some finite number of molecules, especially for lower pressures, that come directly from the plenum.

The gas density was shown above to be inversely proportional to the surface temperature throughout the slot; since the velocity squared is proportional to T_w, the result is a relatively weak dependence of thrust on surface temperature. The thrust does not change with T_w for $P_0 = 49$ Pa. For higher pressures, there was some thrust degradation observed for higher temperatures. The specific impulse slightly increases with pressure, with I_{sp} for $P_0 = 185$ Pa about 4% higher than for $P_0 = 49$ Pa. The ratio of specific impulse values for 573 K to that for 300 K does not depend on pressure and is equal to about 1.34. This is somewhat lower than the theoretical free-molecular value of 1.38.

Table 2. FMMR performance in nitrogen: 2D computations.

P_0, Pa	T_w, K	Mass flow, kg/s	Thrust, N	Isp, s
49	300	$6.7975{\cdot}10^{-7}$	$3.0201{\cdot}10^{-4}$	45.29
49	400	$5.9912{\cdot}10^{-7}$	$3.0287{\cdot}10^{-4}$	51.53
49	500	$5.4257{\cdot}10^{-7}$	$3.0235{\cdot}10^{-4}$	56.80
49	573	$5.1239{\cdot}10^{-7}$	$3.0346{\cdot}10^{-4}$	60.37
69	300	$9.6524{\cdot}10^{-7}$	$4.3337{\cdot}10^{-4}$	45.77
69	400	$8.3901{\cdot}10^{-7}$	$4.2863{\cdot}10^{-4}$	52.08
69	500	$7.5192{\cdot}10^{-7}$	$4.2418{\cdot}10^{-4}$	57.51
69	573	$7.0806{\cdot}10^{-7}$	$4.2421{\cdot}10^{-4}$	61.07
95	300	$1.3343{\cdot}10^{-6}$	$6.0446{\cdot}10^{-4}$	46.18
95	400	$1.1502{\cdot}10^{-6}$	$5.9265{\cdot}10^{-4}$	52.52
95	500	$1.0299{\cdot}10^{-6}$	$5.8689{\cdot}10^{-4}$	58.09
95	573	$9.6222{\cdot}10^{-7}$	$5.8319{\cdot}10^{-4}$	61.78
139	300	$1.9982{\cdot}10^{-6}$	$9.1677{\cdot}10^{-4}$	46.77
139	400	$1.7075{\cdot}10^{-6}$	$8.9177{\cdot}10^{-4}$	53.24
139	500	$1.5112{\cdot}10^{-6}$	$8.7141{\cdot}10^{-4}$	58.78
139	573	$1.4081{\cdot}10^{-6}$	$8.6446{\cdot}10^{-4}$	62.58
185	300	$2.7053{\cdot}10^{-6}$	$1.2521{\cdot}10^{-3}$	47.18
185	400	$2.2717{\cdot}10^{-6}$	$1.1970{\cdot}10^{-3}$	53.71
185	500	$2.0041{\cdot}10^{-6}$	$1.1677{\cdot}10^{-3}$	59.39
185	573	$1.8527{\cdot}10^{-6}$	$1.1473{\cdot}10^{-3}$	63.12

The numerical results for the mass flow as a function of pressure at different chip temperatures is presented in Fig. 8 for two propellants, nitrogen and helium. The DSMC values of stagnation pressure are used here, obtained as an average over all plenum cells. It is clearly seen that in the considered range of pressures, the mass flow is nearly linear for all surface temperatures, $\dot{m} \approx Cp_0$. The proportionality coefficient C is in turn inversely proportional to T_w.

At a fixed pressure, the mass flow strongly depends on the geometry of the chip. Although the shape

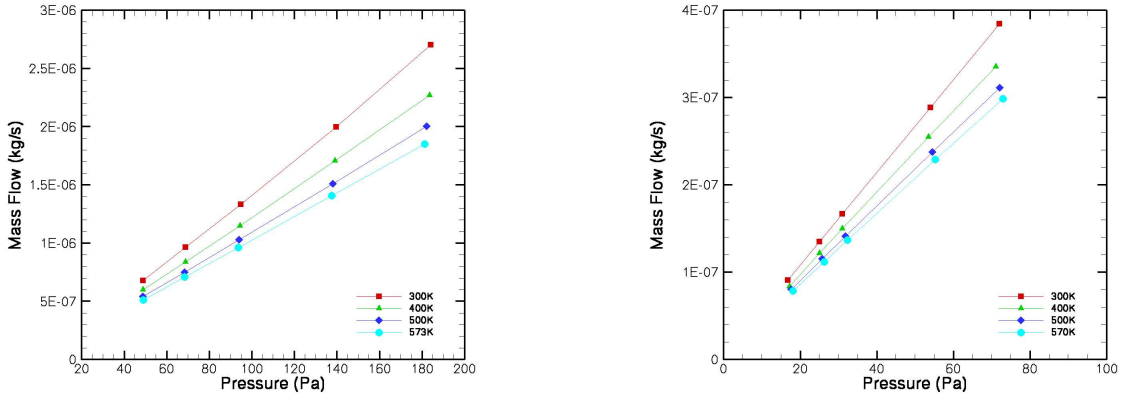

Figure 8. Mass flow of nitrogen (left) and helium (right) *vs* computed plenum pressure for different heater chip temperatures.

of the FMMR slot cross sections is known qualitatively, the uncertainty in the actual dimensions, primarily entrance and exit thickness, is no better than 10%. Moreover, the dimensions may differ for different slots. In addition to this experimental uncertainty, there is a significant numerical uncertainty related to the subsonic boundary conditions. These uncertainties do not allow direct comparison of mass flow and thrust computed as functions of pressure with the corresponding experimental data. They however are expected to be a minor issue for comparison of thrust versus mass flow, since the pressure dependence is weak in this case.

Comparison of the calculated force with the experimental data[5] is given in Fig. 9 for the temperatures 300 K and 573 K. Note that both experimental and numerical thrust values exhibit nearly linear dependence versus mass flow. For nitrogen, the computed thrust is about two percent lower than the experimental values. This is attributed primarily to the impact of the plume molecules backscattered to the outer surface of the heater chip. Such molecules increase the total thrust force, and such an impact is underestimated due to the limitations of the 2D statement of the problem. The impact of the backscattered molecules is larger for helium due to its lower mass and larger back scattering; as a result, the difference between the computed and measured thrust values is somewhat larger for helium.

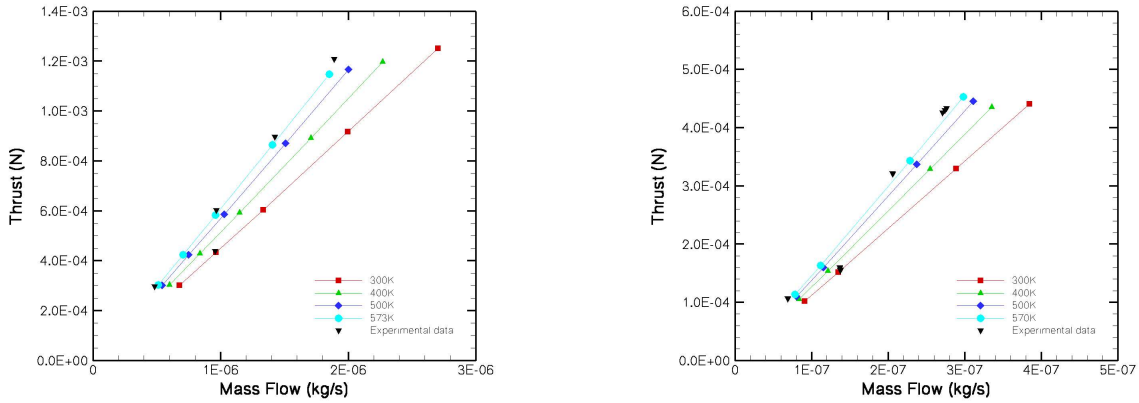

Figure 9. Thrust force in nitrogen (left) and helium (right) *vs* plenum pressure for different heater chip temperatures: comparison with experimental data.

VII. 3D Modeling of the Plenum Flow

As was mentioned above, modeling of the FMMR plume flow has been performed in two steps. First, the flow inside the plenum and in the near field of the plume is calculated. The results are used to specify gas parameters at a starting surface parallel to the outer chip plane 0.5 mm downstream of that plane. The starting surface is utilized in the subsequent modeling of the plume interaction and impingement. Water vapor is used as propellant is these computations.

The results of plenum flow modeling are presented in Fig. 10 where the pressure and temperature fields are shown for $P_0 = 306.5$ Pa and chip temperature of 573 K at the symmetry plane. The figure also illustrates the geometry of the plenum. The gas is supplied through a 6.35 mm tube located at the top left part of the plenum. No significant pressure gradients were observed inside the plenum, with pressure decreasing by less than one percent from the inflow tube to the heater chip. The temperature increases from the inflow value of 300 K to 573 K in the heater region. Note that the increase occurs in the downstream quarter of the plenum, and the temperature is significantly less in the regions close to the top and bottom walls that are kept at 573 K. The temperature is constant inside the slots, and decreases rapidly in the expansion region.

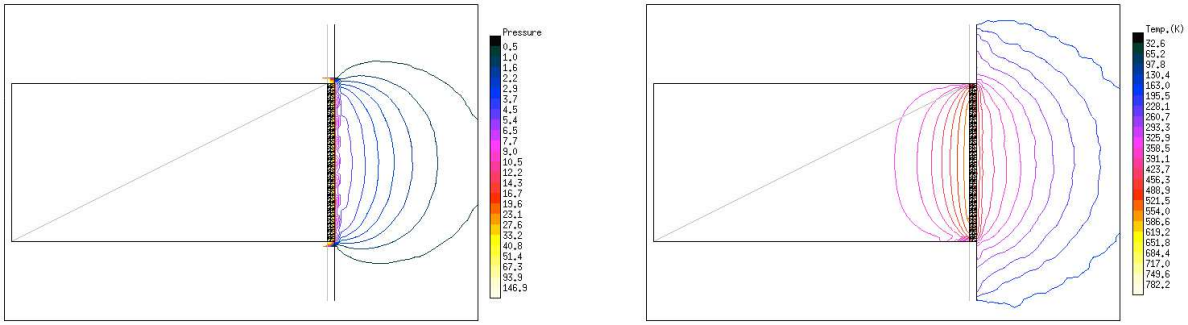

Figure 10. Pressure (Pa) (left) and translational temperature (right) fields inside the plenum for $P_0 = 306.5$ Pa and $T_w = 573$ K.

The flow velocity in the direction perpendicular to the chip is shown in Fig. 11 for two chip temperatures. Similar to the two-dimensional case, the velocity is higher for 573 K, however, the difference is somewhat smaller for the 3D flow. Note also that multiple jets result is velocity isolines being parallel to the chip plane in front of the chip; this flow pattern propagates more than 2 cm downstream.

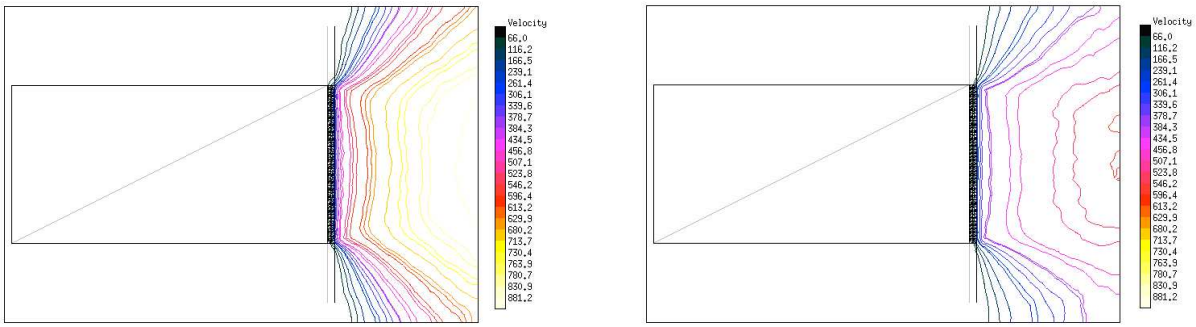

Figure 11. Flow velocity for $T_w = 573$ K (left) and $T_w = 300$ K (right) at $P_0 = 306.5$ Pa.

Let us now examine the impact of chip temperature on the FMMR performance. The performance properties are listed in Table 3 for two plenum pressures and two heater temperatures. In contrast to the

previous 2D runs, the full 3D modeling results in simultaneous decrease in the mass flow and increase in thrust when the temperature increases from 300 K to 573 K. Note that the decrease in the mass flow is lower than the the square root of the temperature ratio. This behavior is attributed to the impact of the cold side walls. The gas is colder than T_w in the downstream corners of the plenum, which in turn causes the larger number density and mass flows in the corner regions.

Comparison of 3D results with the corresponding 2D parameters (rectangular slots were used in these 2D computations to make comparison meaningful) shows the complex 3D flow in the plenum results is significant, about 10%, lower values of both mass flow and thrust. The specific impulse however is close in 2D and 3D computations. Generally, it increases by a factor of 1.34 when the chip temperature goes up, which is the same as in 2D modeling for helium and nitrogen propellants.

Table 3. FMMR performance for water vapor: 3D and 2D simulations.

P_0, N/m^2	Wall Temperature, K	Case	Mass flow, kg/s	Thrust, N	Isp , s
61.3	300	3D	$4.9124 \cdot 10^{-7}$	$2.5970 \cdot 10^{-4}$	53.89
61.3	570	2D	$4.3984 \cdot 10^{-7}$	$3.1847 \cdot 10^{-4}$	73.81
61.3	570	3D	$4.0872 \cdot 10^{-7}$	$2.8756 \cdot 10^{-4}$	71.72
306.5	300	3D	$4.0872 \cdot 10^{-6}$	$1.0957 \cdot 10^{-3}$	54.40
306.5	570	2D	$2.0655 \cdot 10^{-6}$	$1.5605 \cdot 10^{-3}$	77.01
306.5	570	3D	$1.8112 \cdot 10^{-6}$	$1.3034 \cdot 10^{-3}$	73.35

VIII. Modeling of the Plume Expansion Flow

The modeling of the plume expansion and impingement on the spacecraft surface has been performed for the four cases considered in the previous cases and used to compute parameters for the ellipsoidal distribution function at a starting surface located immediately downstream of the heater chip. The general flow field structure is shown in Fig. 12 (left) where the pressure field normalized by the stagnation value is presented in the plane perpendicular to the chip surface and coming through the chip center. Note that it was found that the normalized pressure only weakly depends on gas pressure when decreased from 306.5 Pa to 61.3 Pa and chip temperature when changed from 573 K to 300 K. There is a clearly visible interaction region between the plume and the top surface of the satellite approximately 3 cm downstream from the chip plane. The pressure there is about 50 times higher than that in the corresponding region above the FMMR.

Figure 12 (right) presents the mass flux of water molecules on the surface of the spacecraft. The important conclusion here is that the plume molecules interact only with the top panel of the spacecraft. No molecular flux was registered on the other panels. That means that molecular flux from the plume will be smaller on these surfaces than that from the free stream at LEOs. The mass flux on the top surface is significant, though.

Table 4 shows the values of the total surface mass flow for different flow parameters. The amount of plume molecules that hit the surface is nearly proportional to the plenum pressure. Since the mass flow through the chip decreases with temperature at fixed pressures, the the surface contamination by plume molecules is also lower in this case. Table 4 also gives the total surface force in the direction of the FMMR thrust. It has negative values since the force on the top panel of the spacecraft is much larger than those on the FMMR surfaces, and this large force has a direction opposite to the thrust vector. The last column of the table represents the total force during the operation of FMMR, obtained as a sum of the thrust force (see Table 3) and the surface force. The important conclusion here is that the surface force is comparable in magnitude with the thrust force, which results in about 30% thrust degradation due to the plume-surface interaction.

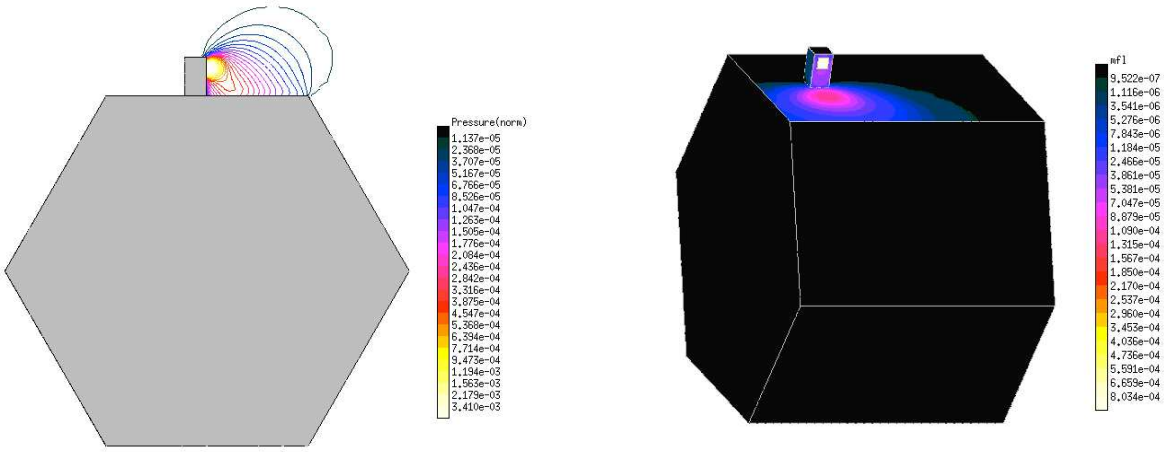

Figure 12. Normalized pressure field (left) and surface mass flux in kg/m^2 (right) for $P_0 = 306.5$ Pa and $T_w = 573$ K.

Table 4. Contamination of spacecraft by FMMR plume

P_0 Pa	Wall Temp. K	Surface Mass flow, kg/s	Surface Force, N	Net Thrust
61.3	300	$1.6628{\cdot}10^{-7}$	$-8.7785{\cdot}10^{-5}$	$1.7191{\cdot}10^{-4}$
61.3	573	$1.3623{\cdot}10^{-7}$	$-9.7307{\cdot}10^{-5}$	$1.9026{\cdot}10^{-4}$
306.5	300	$7.5071{\cdot}10^{-7}$	$-3.8529{\cdot}10^{-4}$	$7.1046{\cdot}10^{-4}$
306.5	573	$6.4807{\cdot}10^{-7}$	$-4.5280{\cdot}10^{-4}$	$8.5057{\cdot}10^{-4}$

IX. Conclusions

The gas flow in a Free Molecule Micro-Resistojet is studied numerically with the direct simulation Monte Carlo method. A 2D flow of nitrogen and helium is modeled through a single heater slot for a qualitatively accurate slot geometry. The results were obtained for a range of plenum pressures from 50 Pa to 200 Pa and chip temperatures from 300 K to 573 K.

The thrust was found to be a weak function of the surface temperature, whereas the mass flow was proportional to the square root of the temperature. The results were compared with available experimental data for thrust vs mass flow. A reasonable agreement of numerical and experimental data was observed. The computed thrust was about 2% lower than experimental for nitrogen, and about 4% for helium. The difference is attributed to the impact of the backscattered plume molecules that act toward increasing thrust; this impact is not properly accounted for in the 2D modeling.

A full 3D modeling of the FMMR geometry has been performed for water vapor in two steps. First, the flow in the plenum was modeled. A significant impact of the cold side walls was found on the FMMR performance parameters compared to the 2D computations. In 3D, the thrust significantly increases with temperature, while the mass flow drop is less significant than in 2D. At the same time, the specific impulse increases with temperature by a factor of 1.34 when the wall temperature increases from 300 K to 573 K both for 2D and 3D.

Second, the FMMR plume flow was computed using starting surface from the first step. The results show that for the present satellite design the contamination is important only for the panel of the satellite where the FMMR is installed. The surface mass flux is negligible for all other panels. The surface force due to the plume-surface interaction is large compared to the thrust force, and the thrust degradation may be as large as 30% for the chip temperature of 573 K.

X. Acknowledgement

This work was supported in part by the Propulsion Directorate of the Air Force Research Laboratory at Edwards Air Force Base, California. The authors thank Taylor Lilly and Riki Lee who provided experimental data for comparison.

References

[1]B. D. Reed, W. de Groot, L. Dang, Experimental Evaluation of Cold Flow Micronozzles, AIAA Paper 2001-3521, July 2001.

[2]D. L. Hitt, C. M. Zakrzwski, and M. A. Thomas, MEMS-based satellite micropropulsion via catalyzed hydrogen peroxide decomposition, *Smart Materials and Structures*, Vol. 10 (2001), pp. 1163-1175.

[3]A. P. London, A. H. Epstein, and J. L. Kerrebrock, High-temperature Bipropellant Microrocket Engine, *J. of Prop. and Power*, Vol. 17, No. 4, July-August 2001.

[4]Ketsdever, A., Green, A., Muntz, E.P., Vargo, S., "Fabrication and Testing of the Free Molecule Micro- Resistojet: Initial Results," AIAA Paper 2000-3672, 36th Joint Propulsion Conference, July 2000.

[5]Lee, R.H., Lilly T.C., Muntz, E.P., Ketsdever, A.D. "Free Molecule Microresistojet: Nanosatellite Propulsion", AIAA Paper 2005-4073.

[6]Ivanov, M.S., Markelov, G.N., Gimelshein, S.F. "Statistical simulation of reactive rarefied flows: numerical approach and applications," *AIAA Paper 98-2669,* June 1998.

[7]Ivanov, M.S., Rogasinsky, S.V., "Analysis of the numerical techniques of the direct simulation Monte Carlo method in the rarefied gas dynamics," *Soviet J. Numer. Anal. Math. Modeling*, Vol. 3, No. 6, 1988, pp. 453-465.

[8]Bird, G.A., *Molecular Gas Dynamics and the Direct Simulation of Gas Flows.* Clarendon Press, Oxford. 458 pp, 1994.